UHASSELT

KNOWLEDGE IN ACTION

Faculteit Wetenschappen

master in materiomics

Masterthesis

Aqueous Solution-Gel Synthesis of Copper-Based Photoelectrode Materials for Photoelectrocatalytic CO_2 Conversion

Gijs Dewitte

Scriptie ingediend tot het behalen van de graad van master in materiomics

PROMOTOR :

Prof. dr. An HARDY

Prof. dr. Marlies VAN BAEL

2024
2025

UHASSELT

KNOWLEDGE IN ACTION

www.uhasselt.be
Universiteit Hasselt
Campus Hasselt:
Martelarenlaan 42 | 3500 Hasselt
Campus Diepenbeek:
Agoralaan Gebouw D | 3590 Diepenbeek

UHASSELT

KNOWLEDGE IN ACTION

Faculteit Wetenschappen

master in materiomics

Masterthesis

Aqueous Solution-Gel Synthesis of Copper-Based Photoelectrode Materials for Photoelectrocatalytic CO_2 Conversion

Gijs Dewitte

Scriptie ingediend tot het behalen van de graad van master in materiomics

PROMOTOR :

Prof. dr. An HARDY

Prof. dr. Marlies VAN BAEL

Aqueous Solution-Gel Synthesis of Copper-Based Photoelectrode Materials for Photoelectrocatalytic CO_2 Conversion

Gijs Dewitte[1,2,3,], Nele Debusschere[1,2,3], Marlies Van Bael[1,2,3], & An Hardy[1,2,3]*

[1] Hasselt University, Institute for Materials Research (imo-imomec), Design and Synthesis of Inorganic Materials (DESINe), Martelarenlaan 42, B-3500 Hasselt, Belgium

[2] imec, imo-imomec, Wetenschapspark 1, B-3590 Diepenbeek, Belgium

[3] Energyville, imo-imomec, Thor Park 8320, B-3600 Genk, Belgium

[*] E-mail: gijs.dewitte@student.uhasselt.be

Keywords: photoelectrochemical CO_2 reduction, photocathode, ternary Cu-La/Y oxide, Cu delafossite, citric acid

Abstract: Photoelectrocatalytic (PEC) CO_2 conversion is a promising strategy for converting CO_2 into value-added chemicals using solar energy directly. The development of suitable photoelectrode materials is critical to enhancing charge transfer, minimizing recombination losses, and thus improving the reaction efficiency. Cuprous delafossite oxides ($CuMO_2$) have garnered significant interest for use as photocathodes due to their p-type conductivity, high hole mobility, and stability. Among them, $CuFeO_2$ has been the most extensively investigated; however, its PEC performance was found to be limited due to significant charge recombination losses. This study investigates the synthesis of two alternative structures, $CuLaO_2$ and $CuYO_2$, in which the Fe^{3+} ion is replaced by La^{3+} and Y^{3+}, respectively. These compounds were synthesized via an aqueous citrate-based solution-gel route, which offers a versatile method for producing various phase-pure, crystalline multi-metal oxides. Compared to alternative synthesis methods, this approach also provides advantages in terms of cost-effectiveness, safety, and environmental sustainability. TGA-DTA and powder XRD were used to gain insight into the underlying mechanisms of the different synthesis steps. Additionally, diffuse reflectance UV-Vis-NIR spectroscopy was employed to characterize the optical properties of the final products.

(Nederlands) Foto-elektrokatalytische (PEC) CO_2-conversie is een veelbelovende strategie om CO_2 rechtstreeks om te zetten in waardevolle chemicaliën met behulp van zonne-energie. De

ontwikkeling van geschikte foto-elektrodematerialen is cruciaal om de ladingsoverdracht te verbeteren, recombinatieverliezen te minimaliseren en zo de reactiesnelheid te verhogen. Koperdelafossietoxiden ($CuMO_2$) hebben aanzienlijke interesse gewekt als fotokathodes vanwege hun p-type geleidbaarheid, hoge gatmobiliteit en stabiliteit. Van deze materialen is $CuFeO_2$ het meest onderzocht; echter, haar PEC-prestaties bleken beperkt te zijn door aanzienlijke ladingsrecombinatieverliezen. In deze studie wordt de synthese onderzocht van twee alternatieve structuren, $CuLaO_2$ en $CuYO_2$, waarbij het Fe^{3+}-ion is vervangen door respectievelijk La^{3+} en Y^{3+}. Deze verbindingen werden gesynthetiseerd via een waterige, citraatgebaseerde *solution-gel*-route, een veelzijdige methode voor het produceren van verscheidene fasezuivere, kristallijne multimetaaloxiden. In vergelijking met alternatieve synthesemethoden biedt deze aanpak ook voordelen op het gebied van kosteneffectiviteit, veiligheid en milieuvriendelijkheid. TGA-DTA en poeder-XRD werden gebruikt om inzicht te verwerven in de onderliggende mechanismen van de verschillende synthesestappen. Daarnaast werd diffuse reflectie UV-Vis-NIR spectroscopie toegepast om de optische eigenschappen van de eindproducten te karakteriseren.

1 Introduction

Carbon capture utilization and storage (CCUS) is regarded as one of the key clean technologies to reduce CO_2 emissions, according to the World Energy Outlook 2024[1] report. By 2050, CCUS should make up about 7% of global CO_2 emissions reduction within this technology mix. For this, the report prescribes an annual CO_2 capture between 3.7 and almost 6 gigatons globally through CCUS, depending on either the Announced Pledges Scenario or the Net Zero Emissions by 2050 Scenario, respectively. Yet, this vision stands in stark contrast to today's reality: in 2024, global CO_2 emissions reached a record 37.8 gigatons, while the current CCUS capacity remains at just about 50 megatons per year. Achieving these targets would demand an approximate 100-fold increase in capacity over the next 25 years.

From a chemical perspective, not only being able to store the captured CO_2 but also to utilize it poses an interesting challenge. This is why much research is being done into materials and technologies for reducing CO_2 into carbon-based value-added chemicals. The opportunity to close the carbon cycle like this opens up a quest for energy-efficient systems to make this conversion possible. Turning to photosynthesis-inspired techniques like photocatalysis (PC)

and photoelectrocatalysis (PEC) instead is especially interesting because they offer the possibility of using sunlight as an energy source directly.

Both techniques require semiconductor (SC) materials with a suitable bandgap (BG) that can absorb incident sunlight and generate high-energy charge carriers.[2, 3] In addition, the conduction band minimum (CBM) should be more negative than one of the possible CO_2 reduction potentials, and the valence band maximum (VBM) more positive than the H_2O oxidation potential[4]; these requirements are illustrated in **Figure 1.1(a)**. For PC systems, which rely solely on sunlight as an energy source, the catalyst material must very strictly meet these conditions, which inherently limits the choice of suitable SC candidates.[3, 4] Furthermore, PC often suffers from electron-hole recombination and conversion selectivity, limiting its conversion efficiency.[4] In contrast, a PEC system benefits from an external bias potential in addition to sunlight harvesting.[2, 4] This bias enhances charge separation and transport by controlling the extent of band bending in the SC, which allows reducing charge recombination and aligning energy levels to drive redox reactions more efficiently.

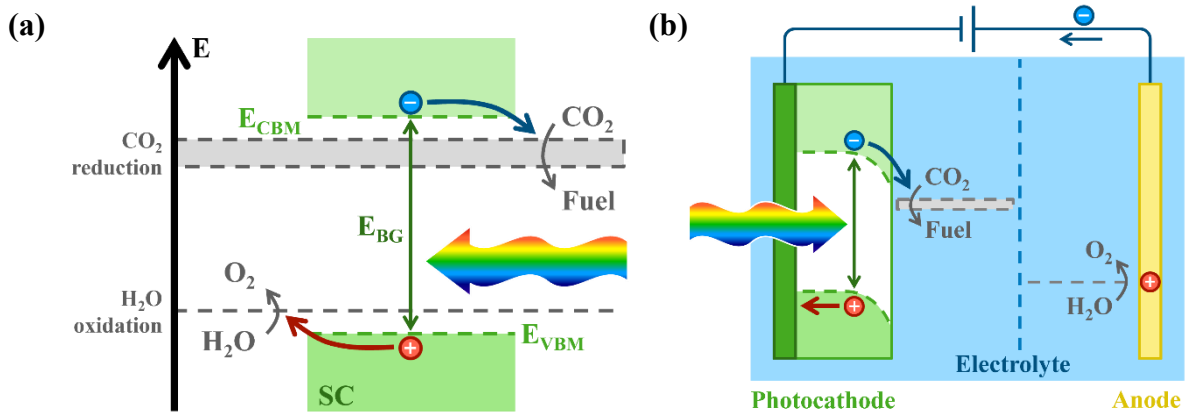

Figure 1.1: (a) Schematic principle of solar-driven CO_2 reduction and (b) a PEC photocathode setup using a p-type semiconductor for this purpose.

PEC systems can employ either a single photocathode, a single photoanode, or a dual photoelectrode setup combining both.[2-4] These photoelectrodes are submerged in a solution in which dissolved CO_2 will undergo reduction under operating conditions. Selectivity remains a critical challenge in catalysts for PEC CO_2 reduction, due to the multitude of possible products that can form through complex reaction pathways[5]; these include carbon monoxide, formic acid, formaldehyde, methanol, methane, and longer-chain organic species, as well as competition with hydrogen evolution. Other material requirements include chemical stability

under operation, strong light absorption, and good charge transport characteristics.[5] Beyond the choice of photoelectrodes, several additional factors significantly influence the performance of PEC CO_2 conversion, including the device architecture, selection of solvent and electrolyte, and the use (or absence) of a membrane.[4]

This study focuses on the synthesis of novel photocathode materials for PEC applications. They consist of a p-type semiconductor, which generates electrons in the conduction band to drive CO_2 reduction reactions and holes in the valence band that facilitate H_2O oxidation at the anode.[3-5] This setup is depicted in **Figure 1.1(b)**. Among the promising candidates for photocathode materials are the cuprous delafossite oxides. These materials have a general formula of $CuMO_2$, where Cu is a monovalent copper ion, Cu^+, and M is a trivalent cation, M^{3+}.[6] **Figure 1.2** depicts the crystal structure, consisting of alternating layers of Cu cations and distorted MO_6 octahedra, which can adopt two polytypes: hexagonal *2H* ($P6_3/mmc$ space group) and rhombohedral *3R* ($R\bar{3}m$ space group). Due to the small difference in formation energies between these polytypes, mixed-phase materials can occur.[7]

The initial interest in copper-based materials for photoelectrodes was driven by studies on Cu_2O, which showed promising results but suffered from severe photocorrosion.[8-10] Consequently, attention shifted to ternary Cu(I) oxides, particularly the Cu delafossite oxides. They exhibit favorable p-type conductivity – a characteristic feature of Cu(I) oxide semiconductors[9] – and a high hole mobility associated with a VBM dominated by hybridization of Cu *d* and O *p* antibonding orbitals[7]. In contrast to Cu_2O, they are much more resistant to corrosion.[8-10] Notably, although the delafossite $CuFeO_2$ is actually metastable in ambient air, it is strongly stabilized in the aqueous electrochemical environments of PEC systems under typical operating conditions; it has an approximate 0.5 V stability window in alkaline solutions.[8]

$CuFeO_2$ is by far the delafossite that has been studied the most for PEC applications. This is due to a combination of advantageous material properties like its narrow optical bandgap of approximately 1.5 eV[8, 9], a high absorption coefficient of up to $\alpha \approx 10^7$ m^{-1}[11], and its CBM being suitably aligned to drive CO_2 reduction reactions[9], as well as its composition of earth-abundant elements. Yet, the experimental photocathodic performance of this material has been underwhelming. There is no general consensus on the exact underlying cause: the problem has been explained by either surface- or bulk-related charge recombination losses.[8, 9, 11] However,

it is likely that it is due to a combination of these effects, with surface recombination believed to be the most significant factor.[12]

This makes it worthwhile to explore the potential of alternative Cu-based delafossites for PEC purposes. The requirement of a trivalent cation, by which the iron ion needs to be replaced, inherently limits the choice of suitable candidates. Therefore, the use of $CuBO_2$, $CuAlO_2$, $CuGaO_2$, $CuScO_2$, $CuCrO_2$, and $CuMnO_2$ for PEC has already been reported.[13] The elements yttrium and lanthanum, belonging to the same group as scandium, form trivalent cations as well; however, there are few, if any, recent reports on the use of $CuYO_2$ and $CuLaO_2$ in this context. Nevertheless, these materials are promising for application as photoelectrocatalysts due to their adequate band gaps[7] and relatively good abundance and low criticality[14, 15] (even though they are considered "rare earth elements"). For these reasons, this thesis focuses on the substitution of Fe^{3+} with La^{3+} and Y^{3+}.

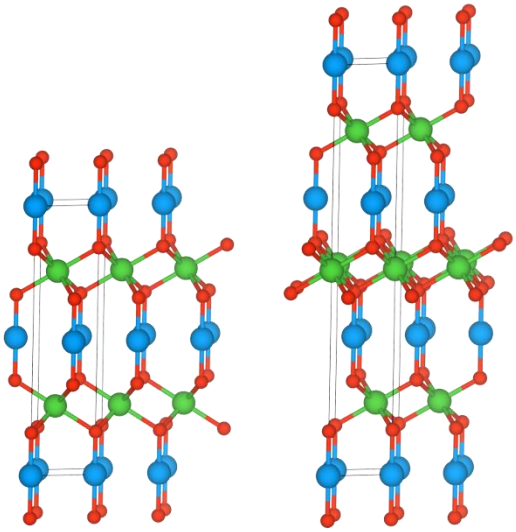

Figure 1.2: Two polytypes of the Cu delafossite crystal structure ($CuMO_2$; Cu^+ = blue, M^{3+} = green, O^{2-} = red): (left) hexagonal *2H* ($P6_3/mmc$) and (right) rhombohedral *3R* ($R\bar{3}m$).[6]

Their metastable nature makes Cu delafossites particularly challenging to synthesize. In recent years, a variety of methods have been used, including sol-gel processes, hydrothermal routes, microwave-assisted techniques, and chemical vapor deposition.[13] However, to tackle the current synthesis challenge, the method of choice is an aqueous citrate-based solution-gel route[16]. This approach starts with the preparation of aqueous precursor solutions in which metal ions form stable citrato complexes. Here lies the first main advantage of the method, namely the precise control over stoichiometry it provides. After accurately determining the

concentrations of the single-metal precursors, these can be mixed with high stoichiometric precision, as is required in the desired multi-metal oxide product. This helps to avoid side phase formation caused by an excess of one of the cations.

The chelating citrato ligands partially shield the positive charge of the cations, thereby significantly suppressing their tendency to undergo hydrolysis.[17] This is crucial for enabling the gradual formation of a glassy gel during solvent evaporation, while preventing the formation of aggregates of individual (hydr)oxides. In this gel, the metal ions are homogeneously distributed within a network of citrate ions. Thanks to their structure with multiple carboxylate groups, citrato ligands enable bridging between metal ions, either by coordinating to multiple cations at once or through non-coordinating carboxylate groups that engage in hydrogen bonding or strong ionic bonding with ammonium.[18] It is this random crosslinking, combined with the increasing solution viscosity upon solvent evaporation, that prevents precipitation of metal citrates and causes the gel to be amorphous in nature instead.

The second main advantage is this ability to ensure homogeneous mixing of the metal ions up to and including the formation of a gel. The gel network effectively locks the metal ions uniformly into place, so that during calcination – *i.e.*, the required decomposition of the gel in an aerobic atmosphere, removing all (nitrogen-containing) organic species and converting it into an oxide – diffusion distances are reduced.[16] It is precisely here that the core strength of this method lies, as this may enable direct crystallization into the multi-metal equilibrium oxide phase, reducing the required processing temperature. Then finally, depending on the thermodynamics of the desired crystalline phase formation or structural properties, additional heat treatments may be needed under specific atmospheric conditions.

However, this method does not unconditionally guarantee preventing chemical phase separation. And once that occurs, the advantages of the process are compromised, as the formation of the target phase would then rely once again on a conventional solid-state reaction. The challenge lies in the fact that phase separation can occur at various stages throughout the synthesis.[18] For instance, insufficient crosslinking during gelation may result in the selective precipitation of metal citrates, a phenomenon influenced by the choice of ligands, the degree of complexation, and the types of pH-dependent complexes present. During calcination, the formation of intermediate phases may occur due to different thermal stabilities of the citrate complexes, which determine their decomposition temperatures. Finally, even if a homogeneous

amorphous oxide is successfully obtained, phase separation can still occur during crystallization. For example, kinetically preferred nucleation at impurities, such as OH^- or trace secondary phases, or suboptimal heating rates may promote segregation. Altogether, this highlights the critical importance of optimizing the solution-gel process to preserve cation homogeneity, in order to fully realize the synthetic advantages it promises.

In addition to the aforementioned benefits, this work exploits this method's versatility for synthesizing the envisioned multi-metal oxides with different compositions and stoichiometries. Moreover, it relies on relatively simple, cheap, and safe starting materials, produces stable precursors under ambient conditions, and uses just water as a solvent, making the process cost-effective, low-risk, and environmentally friendly.[16] However, this last claim deserves some nuance. For instance, citric acid is added solely to be later oxidatively removed again from the gel, resulting in low atom efficiency[19] and emitting CO_2 and other carbon-based volatiles to the air.[20] Moreover, although citric acid is a low-cost, non-toxic, and renewable compound, its production requires large amounts of water, lime, sulfuric acid, and energy, and generates up to 2.5 times its own mass in chemical waste.[21] On the other hand, the solution-gel method itself does not generate any chemical waste, unlike hydrothermal, solvothermal, or sonochemical methods, where it can get as much as several hundred times their product weight.[22] This is due to the use of solvents, including aqueous acidic and alkaline solutions, not only during synthesis but also in subsequent washing steps. Additionally, depending on the target material and appropriate optimizations, this route can be designed for low processing temperatures, making it competitive with alternatives in terms of energy efficiency.[23] And finally, although beyond the scope of this thesis, this method offers the potential for deposition of coatings and thin films from the liquid precursors, allowing for direct processing of materials into functional devices.

In this study, an aqueous citrate-based solution-gel route is developed for the synthesis of $CuLaO_2$ and $CuYO_2$ delafossites. In order to make informed decisions at each stage of the synthesis, it is essential to develop an understanding of the underlying reasons why specific choices lead to particular outcomes. The first focus lies on establishing how to prepare stable Cu, La, and Y precursor solutions that will also enable effective gelation. Next, the decomposition behavior of the resulting gels is investigated using thermal analysis to understand their breakdown mechanisms and to determine appropriate calcination conditions. Furthermore, the influence of calcination and annealing conditions, particularly with respect to

temperature and atmosphere, on the phase formation of the target Cu-La and Cu-Y multi-metal oxides is examined. Finally, the optical properties of a few materials were determined to get a glimpse of their suitability for PEC applications.

2 Materials and methods

2.1 Aqueous metal precursor preparation

In this work, the preparation of copper, lanthanum, and yttrium precursor solutions was developed. Having three separate single-metal precursors allows for more versatility in synthesizing various multi-metal oxides, since the precursors can be mixed to the different required stoichiometries. Precursors of lanthanum and yttrium were prepared at various metal-to-citrate molar ratios (M:Ci) to investigate their effect on solubility and gelation behavior.

To prepare the copper precursor (Cu:Ci (1:1), ~100 mL, ~1 M Cu), 22.564 g of copper(II) formate tetrahydrate ($Cu(HCOO)_2 \cdot 4H_2O$, 98%, Thermo Fisher Scientific) and 19.209 g of anhydrous citric acid ($C_6H_8O_7$, 99%, Sigma-Aldrich) were added to 50 mL of ultrapure water in a 250 mL glass beaker, and stirring the mixture until dissolved. Using a combination pH electrode with an Ag/AgCl reference (Hanna Instruments HI11310), the pH of the solution was raised to pH 7 by adding 25% ammonia solution (NH_3 25%, AnalaR NORMAPUR Analytical Reagent, VWR) under continuous stirring. The beaker was placed in an ice bath during the pH adjustment to avoid excessive heating from the exothermic reaction.

For the lanthanum precursors (La:Ci (1:3), (1:2) and (1:1), ~100 mL, ~0.5 M La), 28.818 g, 12.212 g and 9.606 g of anhydrous citric acid, respectively, were added to 250 mL round-bottom flasks with a minimal required amount of ultrapure water to dissolve the solid substance under continuous stirring. 8.145 g of lanthanum(III) oxide (La_2O_3, 99.99% trace metals basis, Sigma-Aldrich) was stirred into the transparent solutions, dispersing the white powder evenly. Immediate formation of larger chunks was observed, and breaking them down was attempted with vigorous stirring. The white dispersions were refluxed for 2 hours at 100 °C until the whole of the liquid dispersions turned into white solids. These were partially dissolved by adding 25% NH_3 until pH ~9 (MQuant pH-indicator strips (non-bleeding), pH 0 - 14 Universal indicator, Merck Millipore), again gaining white dispersions, though slightly more transparent. The dispersions were refluxed again at 100 °C, but this time for 20 hours to obtain yellow ochre

solutions with a pH between 8 and 9 (strip). Afterwards, the precursors were left to cool down and rest for a couple of days to allow some slight cloudiness to develop. After filtration, the precursors remained transparent.

The yttrium precursors (Y:Ci (1:3) and (1:1), ~100 mL, ~0.5 M Y) were prepared by stirring 5.645 g and 1.882 g of yttrium(III) oxide (Y_2O_3, 99.99% trace metals basis, Sigma-Aldrich), respectively, into the respective citric acid solutions described above. The resulting white dispersions were refluxed for 4 hours at 120 °C to obtain transparent, colorless solutions. The addition of 25% NH_3 caused the transformation of the solutions into similar white solids; the addition was continued until full redissolution and pH ~8 (strip), resulting in transparent, colorless solutions.

Before storage, all precursor solutions were vacuum filtered (Supor Membrane Disc Filters, 0.1 µm - 47 mm, PALL). Their exact metal ion concentrations were determined via inductively coupled plasma optical emission spectroscopy (ICP-OES, PerkinElmer Optima 8300). For this, the precursors were diluted 20,000-fold in a 5% nitric acid solution (HNO_3, prepared from 67 - 69%, BAKER INSTRA-ANALYZED Plus, Avantor) and analyzed against calibration curves prepared from standard solutions of the respective metal ions (Certipur ICP Multi element standard solution IV, Merck Millipore; Lanthanum standard solution, Merck; TraceCERT Yttrium Standard for ICP, Sigma-Aldrich).

2.2 Multi-metal precursor gelation

Based on their determined concentrations, the appropriate volumes of the precursors were combined to the correct stoichiometry for synthesizing the respective multi-metal oxides. In this work, not only were the delafossite phases synthesized, but also in each case a corresponding low-temperature Cu^{2+} oxide – just like $CuFe_2O_4$ alongside $CuFeO_2$ – in order to gain a broader understanding of the phase formation. For $Cu_2Y_2O_5$ and $CuYO_2$, the Cu and Y precursors were mixed to obtain a Cu:Y molar ratio of 1:1. Similarly, $CuLaO_2$ required combining the Cu and La precursors to a Cu:La molar ratio of 1:1; however, for La_2CuO_4, a Cu:La molar ratio of 1:2 was used. All multi-metal precursor solutions were thoroughly mixed for complete homogenization.

To make the metal citrate gels, the precursor mixtures were poured into glass crystallizing dishes and put in a preheated binder oven to dry for 18 hours at 80 °C. Effective gelation resulted in intense blue, transparent, resin-like gels (**Figure S1**). A small piece of every gel (about 5 mg per sample) was chipped off using a metal spatula and saved for thermogravimetric analysis with differential thermal analysis (TGA-DTA, TA Instruments SDT Q600) in dry air to determine their decomposition profiles.

2.3 Calcination

The gels were calcined in two steps based on the TGA-DTA results. A first pre-calcination was performed on them – still in their dishes as such – in a preheated, ventilated oven for 2 hours at 200 °C. Under these conditions, the gels inflated into glossy black domes (**Figure S2**). These pre-calcined products were very brittle and had a porous and flaky inner structure. They were carefully crushed using a spatula and subsequently transferred to a mortar to grind them into fine powders.

The pre-calcined powders were scooped into alumina crucible boats for the second calcination step. Based on the TGA results, Cu_1Y_1 and Cu_1La_1 powders (to make $CuYO_2$ and $CuLaO_2$, respectively) were calcined in a muffle furnace by heating up from room temperature to 450 °C at a rate of 100 °C per hour, holding at 450 °C for 2 hours, and cooling down back to room temperature at 100 °C per hour. Six aliquots of the Cu_1La_2 powder were calcined in a muffle furnace to form La_2CuO_4 directly by heating up from room temperature to either 500, 600 or 700 °C at a rate of 100 °C per hour, holding at those target temperatures for either 2 or 6 hours, and cooling down back to room temperature at 100 °C per hour. One portion of the pre-calcined Cu_1Y_1 powder was analogously calcined in a muffle furnace to form $Cu_2Y_2O_5$, held at a target temperature of 600 °C for 6 hours.

The crystalline phase formation of these seven samples was investigated using powder X-ray diffraction (XRD, Bruker D8, Cu Kα radiation source). A diffuse reflectance UV-Vis-NIR (Agilent Technologies Cary 5000 with DRA 2500 integrating sphere accessory) spectrum was recorded of the 6 hour-700 °C-calcined La_2CuO_4 powder, diluted in potassium bromide (KBr, Uvasol for IR spectroscopy, Merck Millipore). For this, 5 wt% La_2CuO_4 in KBr was used, ground into a homogeneous powder mixture using a mortar and pestle.

2.4 Inert annealing

A high-temperature inert annealing step was necessary for the formation of the delafossite oxide phases out of the 450 °C-calcined Cu_1Y_1 and Cu_1La_1 powders. This final heat treatment was performed by placing the powders in the center of a tube furnace under an inert argon atmosphere. For this, the furnace was flushed with a continuous argon flow 20 minutes prior to the start of the temperature profiles, as well as for its entire duration. To make $CuYO_2$, a sample of the 450 °C-calcined Cu_1Y_1 powder was heated up from room temperature to 800 °C at a rate of 300 °C per hour, held at 800 °C for 10 hours, and cooled back down to room temperature at 300 °C per hour. In the case of $CuLaO_2$, two samples of the 450 °C-calcined Cu_1La_1 powder were heated up from room temperature to either 800 or 1000 °C at a rate of 300 °C per hour, held at those target temperatures for 10 hours, and cooled back down to room temperature at 300 °C per hour. The crystalline phase formation of all the mentioned samples was investigated using powder XRD. A diffuse reflectance UV-Vis-NIR spectrum was measured of the 1000 °C-annealed $CuLaO_2$ powder. For this, the same KBr dilution procedure described before was employed.

3 Results and discussion

3.1 Aqueous metal precursors and gelation

The development of the precursor solutions was carried out to achieve both chemical stability and the formation of homogeneous, transparent gels. For the lanthanum citrate precursor, La:Ci molar ratios of 1:1, 1:2, and 1:3 were investigated. Although the reflux procedure did not yield fully transparent solutions at any ratio, improved dissolution of the filtered solutions was observed with increasing citrate content. For lanthanide (Ln) citrate complexes, hydrolysis is generally only significantly suppressed when the solution contains a Ln:Ci molar ratio of at least 1:2.[24] This corresponds with the poor solubility observed in the current findings at low citric acid content, although it may also be related to the reaction between La_2O_3 and citric acid to form lanthanum citrate, which is promoted by the addition of excess citric acid. In that case, it is not about undissolved La citrate, but unreacted La_2O_3. Also, more stable lanthanum citrate complexes are formed by citrato ligands with increased deprotonation, favored at a high pH. Furthermore, both mononuclear and polynuclear complexes are typically formed with lanthanides. Lanthanum citrate complexes, however, are an exception to this trend, as they tend

to form predominantly mononuclear species stabilized by multiple polydentate chelating citrate ligands, which is also observed in the solid state[25]. Nevertheless, in solid lanthanum citrate, single citrate ligands coordinating to multiple La^{3+} ions also occur, underscoring that structural interpretations based on the solid state must be made with caution when applied to solution chemistry. Only the La:Ci (1:3) was ever used for gelation.

In the case of the yttrium citrate precursor, Y:Ci molar ratios of 1:1 and 1:3 both resulted in clear solutions. However, only the gelation of the Cu_1Y_1 multi-metal precursor, prepared with the Y:Ci (1:3) and Cu:Ci (1:1) precursors (corresponding to an overall metal-to-citrate ratio of 1:2), led to the formation of a homogeneous and transparent gel. Gelation of the Cu_1Y_1 multi-metal precursor based on the Y:Ci (1:1) precursor (overall 1:1) instead resulted in a visually inhomogeneous opaque precipitate, indicating unsuccessful gel formation (**Figure S3**). Based on these findings, La and Y citrate precursors with La:Ci and Y:Ci molar ratios of 1:3 were used consistently in all subsequent experiments to ensure optimal dissolution behavior and effective gelation, while maintaining maximum consistency across experimental conditions.

3.2 Gel decomposition

TGA-DTA was performed on the dried gels of all prepared precursor combinations to investigate their decomposition profiles. This was intended to provide insight into the necessary calcination steps required to remove all carbon and nitrogen-containing matter from the gels. The results are presented in **Figure 3.1**. The TGA and DTA profiles indicate that the gels decompose in two major steps: the first, endothermic one occurs between 170 and 220 °C, and the second, exothermic one between 360 and 410 °C for the Cu_1Y_1 and Cu_1La_1 gels, and between 390 and 440 °C for the Cu_1La_2 gel. The profiles of these current formate-citrate gels are similar to previously explained acetate-citrate gels[20, 26]. During the analysis, the citrate gel network is broken down, going through a complicated series of stages with the formation of distinct decomposition intermediates[27] and evolved volatiles. The initial weight loss is attributed to anaerobic decarboxylation and dehydroxylation of the non-coordinating carboxylate groups and free citrate species. These include ammonium carboxylates and citrates, releasing ammonia and forming intermediate amides. In the case of acetate–citrate gels, acetic acid is evolved during this step as well. Analogously, and based on the decomposition of Cu(II) formate[28], it is expected that formic acid is also released in the present case of the formate-citrate gels. Between the two steep drops, there is a region of more subtle weight loss; likewise,

no pronounced thermal effect is observed in the DTA profile. Now, the metal-ion complexes gradually break down into metal oxides or oxycarbonates (also anaerobically), leaving behind an organic residue. Finally, the second distinct weight loss is ascribed to the oxidative removal of this organic residue, including the amides that had formed.

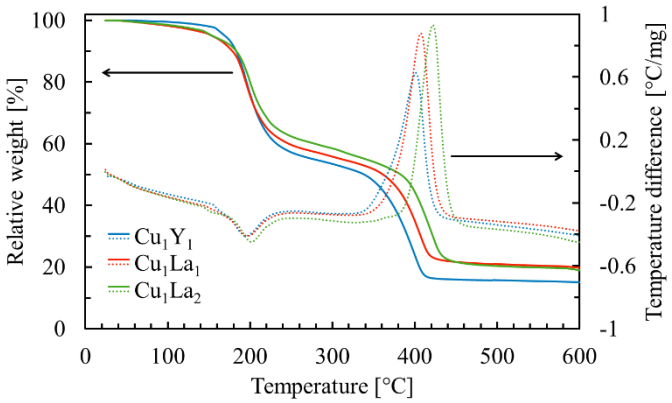

Figure 3.1: TGA-DTA curves showing the decomposition profiles of the Cu_1Y_1, Cu_1La_1, and Cu_1La_2 formate-citrate gels in dry air.

Based on these observations, all gels were initially pre-calcined at 200 °C. This separate pre-calcination step was necessary due to the release of decomposition gases, which causes the gels to expand substantially. It allowed the bulky material to be reduced in volume by grinding it into a powder, making it easier to handle in the subsequent processing steps. Then, the pre-calcined Cu_1Y_1 and Cu_1La_1 powders were calcined at 450 °C. This higher temperature compared to the observed onset temperatures was chosen to ensure complete decomposition, accounting for potential temperature deviations in the muffle furnace. For the Cu_1La_2 powder, calcination was carried out directly to elevated temperatures beyond 450 °C in order to induce crystallization immediately after calcination.

3.3 Cu-La oxides

Six aliquots of the pre-calcined Cu_1La_2 powder were calcined under varying conditions, differing in two durations and three temperatures. The diffraction patterns of the samples held at the target temperature for 2 hours are shown in **Figure 3.2(a)**. These patterns show that La_2CuO_4 begins to form at 600 °C. This is not a spinel-type oxide, analogous to $CuFe_2O_4$, but rather a Ruddlesden-Popper-type perovskite phase[29]. Calcination at 500 °C for 2 hours is insufficient to form this phase; instead, phase separation occurs, resulting in the formation of

the oxycarbonate $La_2O_2CO_3$ alongside CuO. In contrast to the 2-hour calcination, a different phase formation behavior is observed with a 6-hour calcination. As shown in **Figure 3.2(b)**, La_2CuO_4 is already formed at 500 °C after 6 hours at the target temperature.

According to Skakle *et al.*[30] (**Figure S4**), the employed Cu:La molar ratio of 1:2 should result in pure La_2CuO_4 being the only stable oxide phase in ambient air at all these studied temperatures. In fact, it is so all the way up to 1375 °C, where it melts incongruently into La_2O_3 and a liquid phase. The present observation of two separate phases after the 2-hour calcination at 500 °C does not align with this expectation. The calcination process appears to inhibit the direct formation of La_2CuO_4 and instead induces an initial phase separation; in other words, the gel structure does not suffice to maintain homogeneity during decomposition. Prolonged heating, however, seems to allow the separated phases to subsequently react and form the desired La_2CuO_4, as dictated by the thermodynamics represented in the phase diagram.

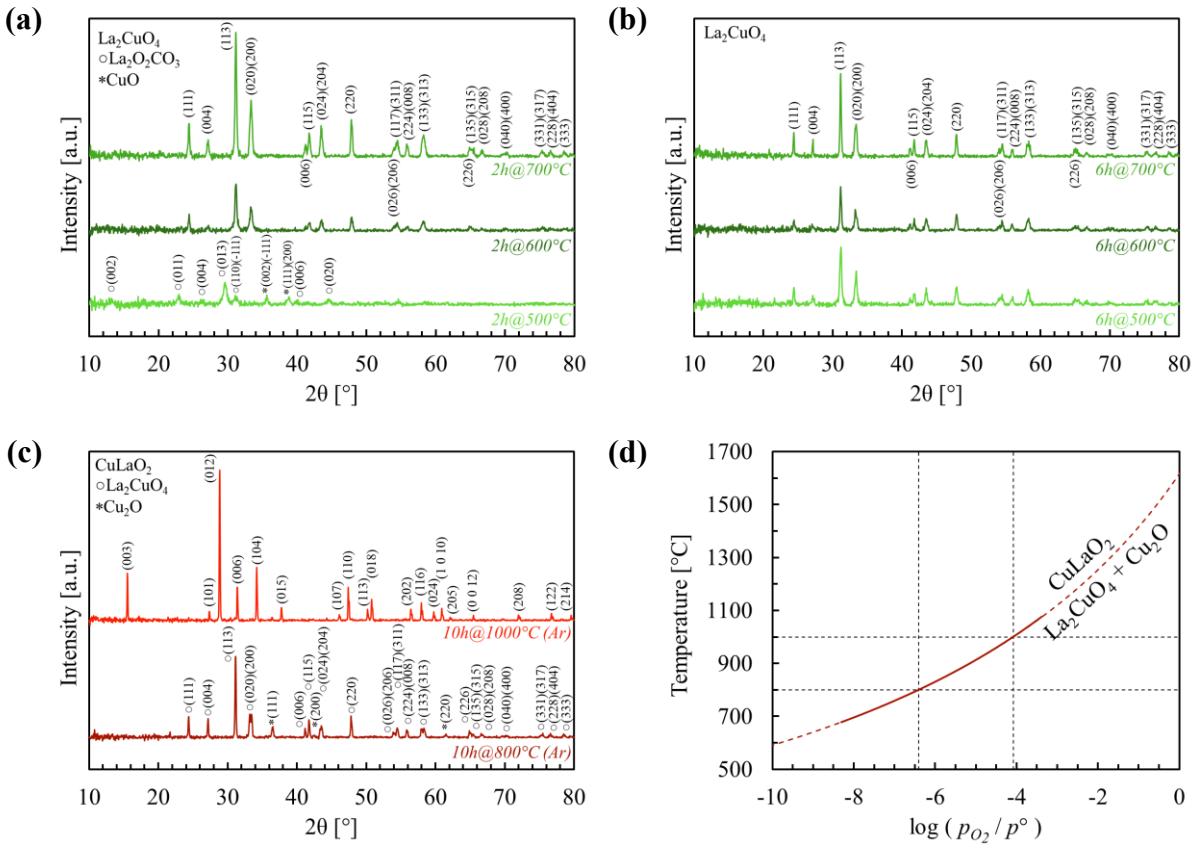

Figure 3.2: Powder XRD patterns of (a) the 2-hour and (b) 6-hour calcined Cu_1La_2 powders in ambient air, and (c) the annealed Cu_1La_1 powders in inert argon atmosphere; (d) T-log($p_{O2}/p°$) curve of the phase equilibrium $8CuLaO_2 + O_2 \rightleftarrows 4La_2CuO_4 + 2Cu_2O$, based on data from Jacob *et al.*[31] (the solid line representing their reported range, the dashed line being an extrapolation of their model).

The calcined Cu_1La_1 powder was subjected to two separate inert annealing treatments at different temperatures. **Figure 3.2(c)** shows that the desired delafossite phase, $CuLaO_2$, is formed at 1000 °C. The diffraction pattern provides evidence for the formation of only the *3R* polytype without the presence of secondary phases. This is surprising, since according to the calculated formation energies of $CuLaO_2$, the *2H* polytype is preferred.[7] In contrast, inert annealing at 800 °C does not result in $CuLaO_2$; instead, the formation of La_2CuO_4 is again observed, along with a Cu_2O secondary phase.

Under these conditions, a Cu:La molar ratio of 1:1 would normally be expected to yield La_2CuO_4 again, accompanied by a CuO side phase. A single-phase $La_2Cu_2O_5$ compound only forms at temperatures above 1002 °C. However, this expected phase behavior applies only under ambient atmospheric conditions and thus differs from the present observations in inert argon atmosphere. Jacob *et al.*[31] investigated the phase formation of Cu–La oxides as a function of oxygen partial pressure (**Figure S5**). For a Cu:La ratio of 1:1, the La_2CuO_4 and CuO mixture is stable at 927 °C down to an oxygen partial pressure of $\log(p_{O2}/p°) = -1.545$, below which the CuO component is reduced to Cu_2O. Below $\log(p_{O2}/p°) = -4.84$, the La_2CuO_4 and Cu_2O mixture reacts to form the delafossite phase $CuLaO_2$, which in turn remains stable until $\log(p_{O2}/p°) = -7.58$, beyond which it is reduced further to Cu and La_2O_3. There appears to be a sequence of successive reactions as described in **Equation 3.1**, with equilibrium states established at the aforementioned oxygen partial pressures. Lowering the partial pressure below each equilibrium value shifts the equilibrium progressively to the right.

$$4La_2CuO_4 + 4CuO \rightleftarrows 4La_2CuO_4 + 2Cu_2O + O_2 \rightleftarrows 8CuLaO_2 + 2O_2 \rightleftarrows 8Cu + 4La_2O_3 + 4O_2 \quad (3.1)$$

$$8CuLaO_2 + O_2 \rightleftarrows 4La_2CuO_4 + 2Cu_2O \quad (3.2)$$

$$\frac{\Delta\mu_{O_2}}{\mathrm{J\cdot mol^{-1}}} = -304\,620 + 161.21 \cdot \frac{T}{\mathrm{K}} \quad (3.3)[31]$$

$$\mu_{O_2} = \mu°_{O_2} + R \cdot T \cdot \ln\left(\frac{p_{O_2}}{p°}\right) \quad (3.4)$$

$$\frac{T}{\mathrm{K}} = \frac{-304\,620}{19.145 \cdot \log\left(\frac{p_{O_2}}{p°}\right) - 161.21} \quad (3.5)$$

Moreover, the same authors established a relationship for the reaction in **Equation 3.2** between the oxygen chemical potential and temperature, as expressed in **Equation 3.3**, which is relevant to the phase formation studied in the present work. Using **Equation 3.4**, Equation 3.3 can be rewritten as **Equation 3.5**, which is plotted in **Figure 3.2(d)**. This curve represents a T-$\log(p_{O2}/p°)$ equilibrium line indicating the temperature and oxygen partial

pressure conditions under which the equilibrium described in Equation 3.2 is established. Just above the curve, $CuLaO_2$ forms; just below it, La_2CuO_4 and Cu_2O are the stable phases. With this, it is important to note that Figure 3.2(d) does not provide information on other competing equilibria and is therefore not a phase diagram. Nonetheless, it allows the current results to be explained under the assumption that they occurred at $\log(p_{O2}/p°)$ below - 4.0 and above - 6.4, enabling the formation of $CuLaO_2$ at 1000 °C, but not at 800 °C, respectively. This would mean that the employed argon atmosphere was not entirely free of oxygen. An alternative explanation could be that annealing at 800 °C was kinetically limited and that the duration was insufficient for the reaction to proceed to completion. Most importantly, the equation implies that the equilibrium shifts to lower temperatures at lower oxygen partial pressures, which is more clearly visualized by extrapolating the curve beyond the reported range of data. Practically for the current material synthesis investigation, this suggests that the minimum required annealing temperature could potentially be lowered by further reducing the oxygen partial pressure in the annealing atmosphere.

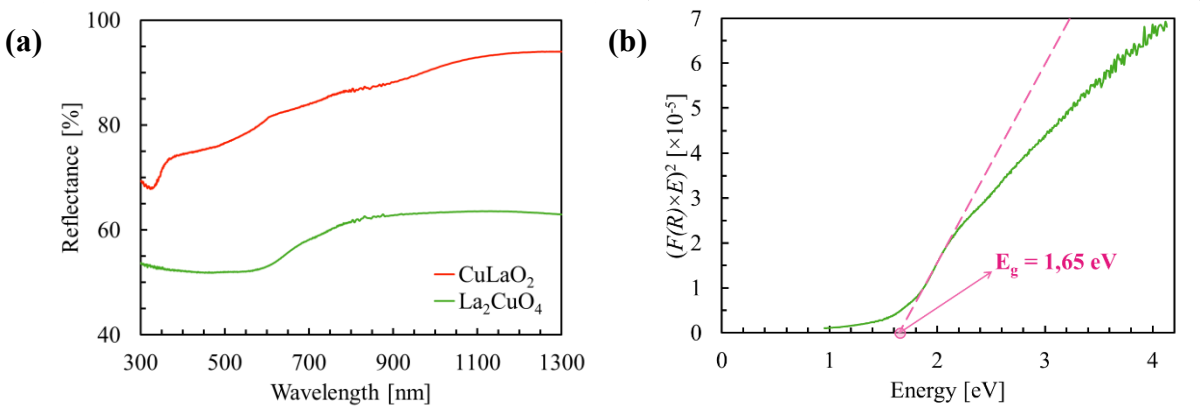

Figure 3.3: (a) Diffuse reflectance UV-Vis-NIR spectra of the $CuLaO_2$ and La_2CuO_4 powders and (b) the Tauc plot of the La_2CuO_4 spectrum.

To gain insight into the optical properties of the synthesized La_2CuO_4 and $CuLaO_2$, diffuse reflectance UV-Vis-NIR spectra were recorded for the respective powders. The results are shown in **Figure 3.3(a)**. The spectrum of La_2CuO_4 exhibits a clear drop in reflectance, characteristic of typical semiconductor behavior: wavelengths shorter than the band gap are absorbed, while longer wavelengths are reflected. **Figure 3.3(b)** illustrates how a Tauc plot[32] was used to determine the band gap of the material, based on the Kubelka-Munk function[33] of the spectral data. The x-intercept of the straight line fitted to the linear region of the function corresponds to the band gap energy. Using this method, the band gap of the present sample was

determined to be 1.65 eV, which is in good agreement with a recently reported experimental value of 1.6 eV[29]. This bandgap allows for the absorption of a substantial part of the solar spectrum.

The reflectance spectrum of the synthesized $CuLaO_2$ appears quite different. Unlike La_2CuO_4, there is no distinct drop in reflectance; instead, a more gradual attenuation is observed with decreasing wavelength. It is unclear whether this result is due to the intrinsic optical behavior of the material or influenced by the nature or preparation of the sample. When the Kubelka-Munk function was applied, no clearly defined linear regions were observed, making it difficult to determine one or more band gaps. Several theoretical studies on this material report band gaps ranging from 2.35 to 2.75 eV.[7, 34-36] Also, an experimental value of 2.34 eV has been reported[37], although the author did not provide supporting evidence in their publication. In any case, there is no distinct feature in the present spectrum to which any of these values can be linked.

3.4 Cu-Y oxides

From the pre-calcined Cu_1Y_1 powder, both a calcined and an inert-annealed final product were prepared. **Figure 3.4** shows that calcination for 6 hours at 600 °C resulted in the formation of $Cu_2Y_2O_5$. According to Gadalla *et al.*[38] (**Figure S6**), the employed Cu:Y molar ratio of 1:1 should lead to $Cu_2Y_2O_5$ being the only stable oxide phase in ambient air at 600 °C. In fact, this phase remains stable up to 1110 °C, where it melts incongruently into Y_2O_3 and a liquid phase. However, the presence of secondary phases Y_2O_3 and CuO was also observed, although thermodynamically, it should not be possible for these three phases to coexist in any Cu:Y molar ratio. As observed previously with the pre-calcined Cu_1La_2 powder, the calcination process appears to induce an initial phase separation, with prolonged heating allowing the distinct phases to react and form $Cu_2Y_2O_5$. The current experiment involving a 6-hour calcination may not have been sufficient for that reaction to reach completion.

Inert annealing of the 450 °C-calcined Cu_1Y_1 powder resulted in the formation of $CuYO_2$. Unlike $CuLaO_2$, however, a mixture of the two delafossite polytypes was observed. As with $CuLaO_2$, phase formation under these conditions cannot be explained using phase studies conducted in ambient air. Zhang *et al.*[39] investigated the phase behavior of Cu-Y oxides under reduced oxygen partial pressures (**Figure S7**). For a Cu:Y molar ratio of 1:1 at an oxygen

pressure of 0.1 bar, the $Cu_2Y_2O_5$ phase remains stable up to 1076 °C, at which point it converts to the delafossite phase according to **Equation 3.6**. This phase remains stable up to 1140 °C, after which it melts incongruently into Y_2O_3 and a liquid phase. In their study on the temperature-oxygen pressure relationship for this stoichiometry, they found that $CuYO_2$ formation becomes possible below an oxygen partial pressure of 0.17 bar. At this pressure and a temperature of 1110 °C, a ternary phase equilibrium is established, in which $Cu_2Y_2O_5$, $CuYO_2$, and Y_2O_3 + liquid coexist. At lower oxygen pressures, the equilibrium temperature for the reaction described in Equation 3.6 decreases, similar to what was observed for the reaction in Equation 3.2. Although their experimental data do not extend far enough to provide direct evidence for the current results, extrapolation of their findings suggests that the formation of $CuYO_2$ is indeed plausible under the present conditions of reduced oxygen partial pressure and temperature, analogous to the behavior of Cu-La oxides.

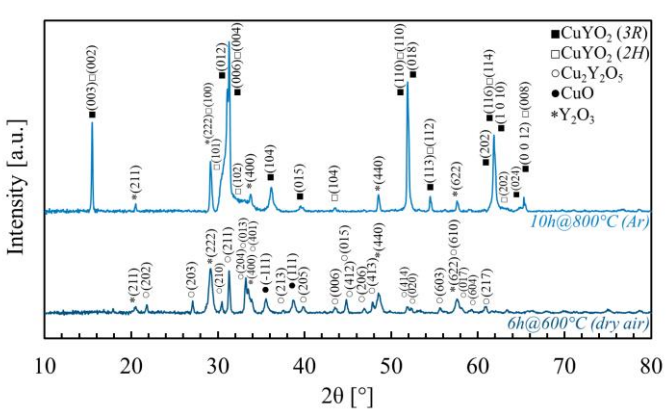

Figure 3.4: Powder XRD patterns of the Cu_1Y_1 powders, calcined in dry air and annealed in inert argon atmosphere.

$$2Cu_2Y_2O_5 \rightleftarrows 4CuYO_2 + O_2 \tag{3.6}$$

Additionally, a Y_2O_3 secondary phase appears to be present in this sample, although in this case, neither the presence of CuO nor Cu_2O was observed. The coexistence of $CuYO_2$ and Y_2O_3 is, in fact, thermodynamically possible under the right conditions, provided that there is a molar excess of Y relative to Cu, however. This would imply that the analyzed sample did not consist of a stoichiometric 1:1 Cu:Y mixture, or that there might be an amorphous Cu-containing phase present. However, this interpretation should be considered preliminary, as the reproducibility still needs to be verified.

4 Conclusion and outlook

This study established an aqueous solution-gel route for preparing multi-metal Cu-La and Cu-Y oxide phases. It elucidates key relationships between precursor composition, gelation behavior, gel decomposition, and phase formation, and demonstrates that careful tuning of synthetic conditions enables the targeted synthesis of various oxide materials, including the rather challenging delafossite phases and related low-temperature Cu^{2+} oxide phases.

A set of single-metal citrate precursor solutions of Cu, La, and Y was developed. The effect of metal-to-citrate (M:Ci) ratios on precursor solubility and gelation was evaluated, with La:Ci and Y:Ci molar ratios of 1:3 found to offer optimal solubility and gel transparency, ensuring consistent and effective gelation when combined with Cu:Ci (1:1) solutions. TGA-DTA revealed that the decomposition of these gels proceeds in two major steps. This insight determined the choice of a two-step calcination approach for the complete removal of all carbon- and nitrogen-based matter.

Next, phase formation in the Cu-La and Cu-Y oxide systems was investigated. By selecting appropriate synthesis conditions, the formation of La_2CuO_4, $Cu_2Y_2O_5$, and the delafossites $CuLaO_2$ and $CuYO_2$ was achieved. It was found that a combination of the heat treatment's duration, temperature, and atmosphere plays a decisive role in phase formation, not only in terms of thermodynamic stability but also in determining the extent to which the reactions are able to proceed. In several instances, calcination was observed to induce phase separation. However, this never prevented the successful formation of the desired phases within the scope of the present experiments. Literature on phase studies was consulted to help explain the behavior observed during delafossite formation. Notably, it was found that the minimum annealing temperature required for delafossite formation is highly dependent on the oxygen partial pressure.

Looking ahead, the successful formation of La_2CuO_4 after just 6 hours of calcination at 500 °C suggests promising prospects for direct thin-film deposition on transparent conductive oxide (TCO)-coated glass substrates. This enables relatively straightforward fabrication of functional photoelectrodes for PEC applications. In contrast, the delafossite phases $CuLaO_2$ and $CuYO_2$ required much higher synthesis temperatures – 1000 °C and 800 °C, respectively – which currently limits their suitability in direct thin-film approaches. Nevertheless, functional

photoelectrodes could potentially be fabricated by mechanically milling the synthesized powders (*e.g.*, via bead milling) to a suitable particle size and then depositing them through a suspension on a substrate. Special care must be taken to preserve the crystallinity of the materials during such processing.

Although direct film deposition appears infeasible for $CuLaO_2$ and $CuYO_2$ under current synthesis conditions, there is significant potential for further synthesis optimization. Adjustments such as altering the atmospheric conditions and the annealing duration, combined with exploring alternative substrate materials, may lead to reducing annealing temperatures enough to enable direct deposition. *In situ* characterization techniques such as high-temperature XRD or Raman spectroscopy could provide valuable insights by tracking phase formation and transitions in real-time during thermal treatment.

Finally, future research should focus on the application and characterization of these materials as photoelectrocatalysts. This includes integrating the synthesized oxides into a PEC system, illuminated with simulated sunlight, in order to evaluate their performance and stability in various electrolytes. Process parameters should be optimized to maximize conversion efficiency. Comprehensive characterization of the resulting thin films is also essential. This should include techniques such as XRD for phase identification and grain size analysis; UV-Vis-NIR spectroscopy for optical properties; atomic force microscopy (AFM) and scanning electron microscopy with energy dispersive X-ray spectroscopy (SEM-EDX) for surface morphology and compositional uniformity; and X-ray or ultraviolet photoelectron spectroscopy (XPS/UPS) in combination with Mott–Schottky electrochemical impedance spectroscopy (MS-EIS) to determine band positions and charge carrier densities. By correlating structural, optical, and electronic properties with PEC performance, a deeper understanding can be gained of the mechanisms driving catalytic activity and selectivity. This knowledge will ultimately contribute to the development of high-performance photocathodes for CO_2 valorization, moving further towards scalable and sustainable artificial photosynthesis.

Acknowledgements

First and foremost, my profound gratitude goes to my supervisor, Nele Debusschere, MSc, and my promoters, Professor Dr An Hardy and Professor Dr Marlies Van Bael, for their support during this research project and for the valuable learning experience it provided. In addition, I

would like to thank the members of the DESINe group's PEC team for the fruitful discussions and exchange of ideas concerning the continuation of my lab work; they include Nele Debusschere, MSc, Kristy Talukdar, MSc, Mr. Robbe Jacops, MSc, Dr Bjorn Joos, and Dr Ken Elen. Finally, special thanks go to all the researchers who carried out the analyses of my prepared samples, providing me with the most essential information for this thesis: ICP-OES by Elsy Thijssen, MSc, TGA by Dr *ir* Dries De Sloovere, and XRD by Nele Debusschere, MSc, Naomi Billiet, MSc, and Hanne Broux, MSc.

References

[1] IEA, *World Energy Outlook 2024*. 2024, OECD Publishing: Paris.

[2] Bessegato, G.G., et al. Achievements and Trends in Photoelectrocatalysis: from Environmental to Energy Applications. *Electrocatalysis* **2015**, *6* (5), 415-441.

[3] Kalamaras, E., et al. Solar Carbon Fuel via Photoelectrochemistry. *Catalysis Today* **2018**, *317*, 56-75.

[4] Pawar, A.U., et al. General Review on the Components and Parameters of Photoelectrochemical System for CO_2 Reduction with in Situ Analysis. *ACS Sustainable Chemistry & Engineering* **2019**, *7* (8), 7431-7455.

[5] Putri, L.K., et al. Toward Excellence in Photocathode Engineering for Photoelectrochemical CO_2 Reduction: Design Rationales and Current Progress. *Advanced Energy Materials* **2022**, *12* (41), 2201093.

[6] Marquardt, M.A., N.A. Ashmore, and D.P. Cann. Crystal Chemistry and Electrical Properties of the Delafossite Structure. *Thin Solid Films* **2006**, *496* (1), 146-156.

[7] Huda, M.N., et al. Group-IIIA versus IIIB Delafossites: Electronic Structure Study. *Physical Review B* **2009**, *80* (3), 035205.

[8] Ferri, M., et al. Thermodynamic Stability and Native Point Defects of $CuFeO_2$ Photocathodes in Dry and Electrochemical Environments. *The Journal of Physical Chemistry C* **2019**, *123* (49), 29589-29598.

[9] Jiang, C.-M., et al. Electronic Structure and Performance Bottlenecks of $CuFeO_2$ Photocathodes. *Chemistry of Materials* **2019**, *31* (7), 2524-2534.

[10] Präg, R., et al. Photoelectrochemical Properties of $CuFeO_2$ Photocathodes Prepared by Pulsed Laser Deposition. *Chemistry of Materials* **2024**, *36* (16), 7764-7780.

[11] Prévot, M.S., et al. Evaluating Charge Carrier Transport and Surface States in $CuFeO_2$ Photocathodes. *Chemistry of Materials* **2017**, *29* (11), 4952-4962.

[12] Boudoire, F., et al. Spray Synthesis of $CuFeO_2$ Photocathodes and In-Operando Assessment of Charge Carrier Recombination. *The Journal of Physical Chemistry C* **2021**, *125* (20), 10883-10890.

[13] Hossain, S.A., et al. Synthesis, Characterization, and Application of Delafossites as Catalysts for Degrading Organic Pollutants and Degradation Mechanisms: A Detailed Insight. *Surfaces and Interfaces* **2023**, *42*, 103281.

[14] Binnemans, K., et al. Rare Earths and the Balance Problem: How to Deal with Changing Markets? *Journal of Sustainable Metallurgy* **2018**, *4* (1), 126-146.

[15] Balaram, V. Rare earth elements: A review of applications, occurrence, exploration, analysis, recycling, and environmental impact. *Geoscience Frontiers* **2019**, *10* (4), 1285-1303.

[16] Van Bael, M.K., A. Hardy, and J. Mullens. Aqueous Precursor Systems. In *Chemical Solution Deposition of Functional Oxide Thin Films*, T. Schneller, et al. Eds.; Springer Vienna, 2013; pp 93-140.

[17] Danks, A.E., S.R. Hall, and Z. Schnepp. The Evolution of 'Sol–Gel' Chemistry as a Technique for Materials Synthesis. *Materials Horizons* **2016**, *3* (2), 91-112, 10.1039/C5MH00260E.

[18] Narendar, Y. and G.L. Messing. Mechanisms of Phase Separation in Gel-Based Synthesis of Multicomponent Metal Oxides. *Catalysis Today* **1997**, *35* (3), 247-268.

[19] Marchal, W., et al. Precursor Design Strategies for the Low-Temperature Synthesis of Functional Oxides: It's All in the Chemistry. *Chemistry – A European Journal* **2020**, *26* (42), 9070-9083.

[20] Hardy, A., et al. Study of the Decomposition of an Aqueous Metal–Chelate Gel Precursor for $(Bi,La)_4Ti_3O_{12}$ by means of TGA–FTIR, TGA–MS and HT-DRIFT. *Thermochimica Acta* **2003**, *397* (1), 143-153.

[21] Binnemans, K. and P.T. Jones. Lindy Effect in Hydrometallurgy. *Journal of Sustainable Metallurgy* **2025**.

[22] Ordoñez, M.F., et al. Paving the Green Path: a Novel Approach to Material Manufacturing using LCA. *Chemical Engineering Journal Advances* **2023**, *16*, 100575.

[23] Lee, S.-S. and T.-W. Hong. Life Cycle Assessment for Proton Conducting Ceramics Synthesized by the Sol-Gel Process. *Materials* **2014**, *7* (9), 6677-6685.

[24] Guseva, P.B., et al. Complexation of Lanthanide Ions with Citric Acid in Aqueous Solutions. *Russian Journal of General Chemistry* **2023**, *93* (12), 3135-3142.

[25] Vanhoyland, G., et al. Characterization and Structural Study of Lanthanum Citrate Trihydrate $[La(C_6H_5O_7)(H_2O)_2]\cdot H_2O$. *Journal of Solid State Chemistry* **2005**, *178* (1), 166-171.

[26] Nelis, D., et al. Synthesis of Strontium Bismuth Niobate ($SrBi_2Nb_2O_9$) using an Aqueous Acetate–Citrate Precursor Gel: Thermal Decomposition and Phase Formation. *Thermochimica Acta* **2005**, *426* (1), 39-48.

[27] Fischer, J.W., L.H. Merwin, and R.A. Nissan. NMR Investigation of the Thermolysis of Citric Acid. *Applied Spectroscopy* **1995**, *49* (1), 120-126.

[28] Marchal, W., *Redox Mechanisms in Low-Temperature Solution Processing of Materials for Flexible Electronics*. 2018.

[29] Parida, S., et al. Spin Coated La_2CuO_4 Thin Film: an Extensive Study on Optical Dispersion Parameters. *Optik* **2023**, *278*, 170728.

[30] Skakle, J.M.S. and A.R. West. Subsolidus Relations in the La_2O_3─CuO─CaO Phase Diagram and the La_2O_3─CuO Binary Join. *Journal of the American Ceramic Society* **1994**, *77* (8), 2199-2202.

[31] Jacob, K.T. and K.P. Jayadevan. Phase Relations in the System Cu-La-O and Thermodynamic Properties of $CuLaO_2$ and $CuLa_2O_4$. *Journal of Materials Science* **2002**, *37* (8), 1611-1620.

[32] Makuła, P., M. Pacia, and W. Macyk. How To Correctly Determine the Band Gap Energy of Modified Semiconductor Photocatalysts Based on UV–Vis Spectra. *The Journal of Physical Chemistry Letters* **2018**, *9* (23), 6814-6817.

[33] Landi, S., et al. Use and Misuse of the Kubelka-Munk Function to Obtain the Band Gap Energy from Diffuse Reflectance Measurements. *Solid State Communications* **2022**, *341*, 114573.

[34] Liu, Q.-J., et al. Structural, Mechanical, Electronic, Optical Properties and Effective Masses of $CuMO_2$ (M = Sc, Y, La) Compounds: First-Principles Calculations. *Solid State Sciences* **2014**, *31*, 37-45.

[35] Azmat Ali, M., et al. First Principles Study of Cu Based Delafossite Transparent Conducting Oxides $CuXO_2$ (X=Al, Ga, In, B, La, Sc, Y). *Materials Science in Semiconductor Processing* **2015**, *38*, 57-66.

[36] Khedidji, M., et al. Electronic Structure, Phonons, and Born Effective Charges in $CuLaO_2$: a First-Principles Study. *Solid State Communications* **2024**, *394*, 115733.

[37] Koriche, N., A. Bouguelia, and M. Trari. Photocatalytic Hydrogen Production over New Oxide $CuLaO_{2.62}$. *International Journal of Hydrogen Energy* **2006**, *31* (9), 1196-1203.

[38] Gadalla, A.M. and P. Kongkachuichay. Compatible phases of the Y_2O_3–CuO–Cu_2O system in air. *Journal of Materials Research* **1991**, *6* (3), 450-454.

[39] Zhang, W. and K. Osamura. Oxygen Pressure Dependence of the Cu_2O-CuO-Y_2O_3 Phase Diagram / Die Sauerstoffpartialdruck-Abhängigkeit des Phasendiagramms Cu_2-O-CuO-Y_2O_3. *International Journal of Materials Research* **1990**, *81* (3), 196-201. (acccessed 2025-05-28).

Supporting information

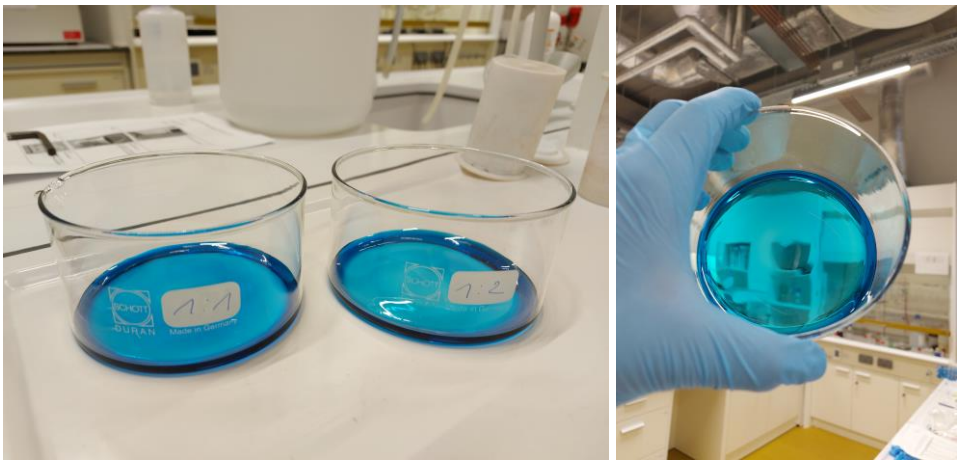

Figure S1: Dried multi-metal formate-citrate gels.

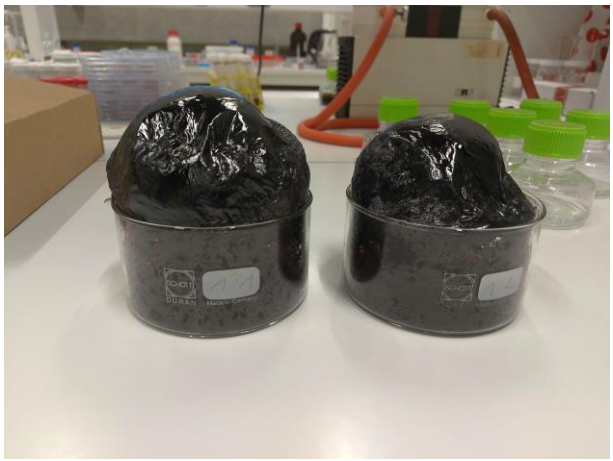

Figure S2: Inflated pre-calcined multi-metal product.

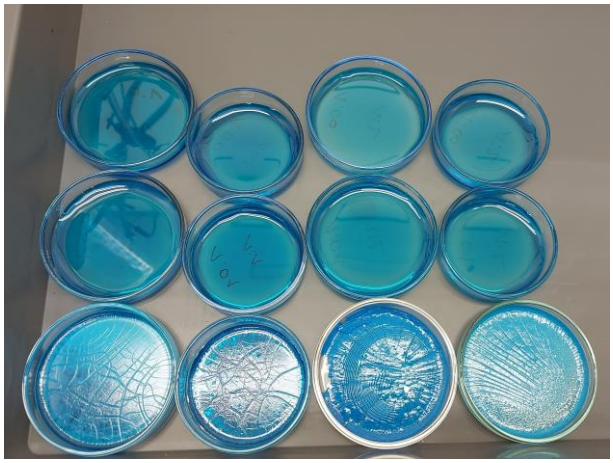

Figure S3: Gelation variation of the Cu_1Y_1 gels: top two rows prepared with the Y:Ci (1:3) precursor (total M:Ci of 1:2), bottom row prepared with the Y:Ci (1:1) precursor (total M:Ci of 1:1).

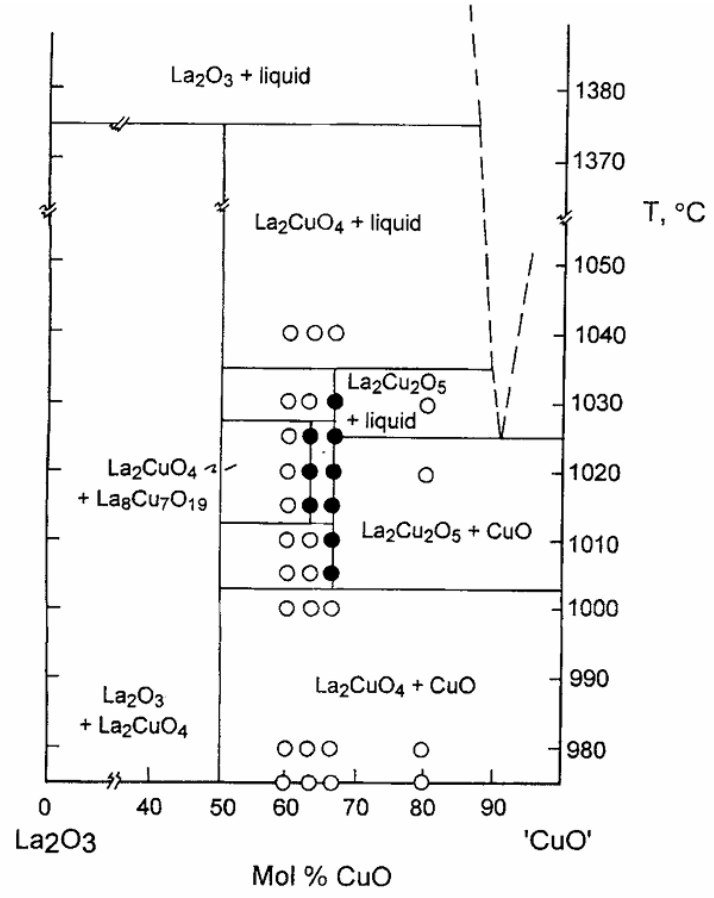

Fig. 1. Proposed phase diagram for the La_2CuO_4–CuO binary system ((- - -) estimated locus of the liquidus, (●) single-phase samples, and (○) phase mixtures).

Figure S4: Temperature-composition Cu-La oxide phase diagram in air (from Skakle *et al.*[30]).

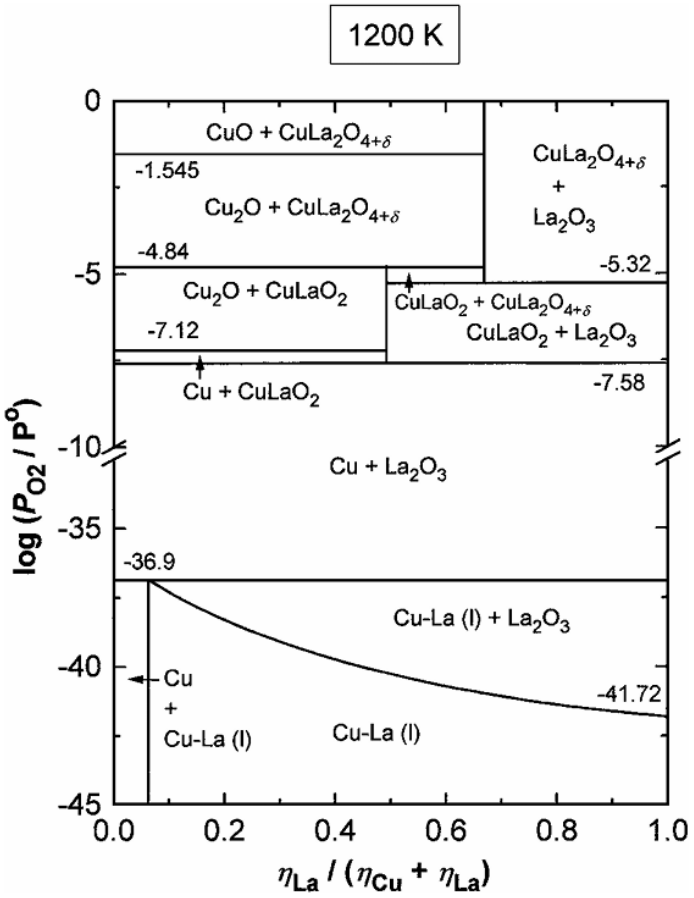

Figure 11 Oxygen chemical potential diagram for the system Cu-La-O at 1200 K composed from the results obtained in this study and data on binary phases reported in the literature [30, 31, 33, 34].

Figure S5: Oxygen pressure-composition Cu-La oxide phase diagram at 1200 K (from Jacob *et al.*[31]).

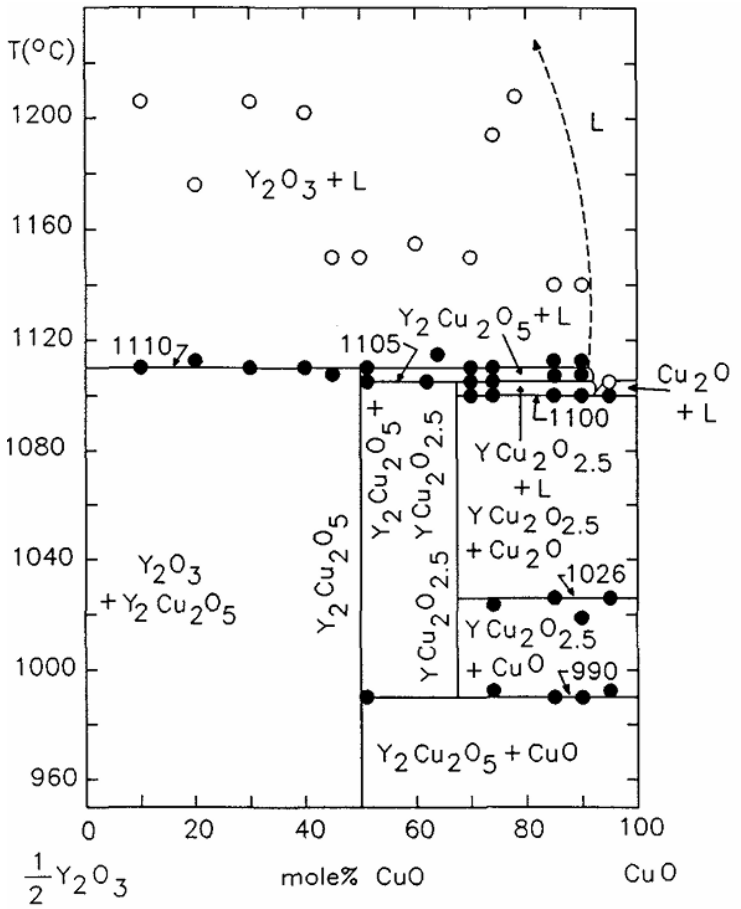

FIG. 2. Pseudo-binary phase diagram of the Y_2O_3–CuO system in air (the indicated condensed phases are all in equilibrium with air): (●) phase change and (○) partial melting.

Figure S6: Temperature-composition Cu-Y oxide phase diagram in air (from Gadalla *et al.*[38]).

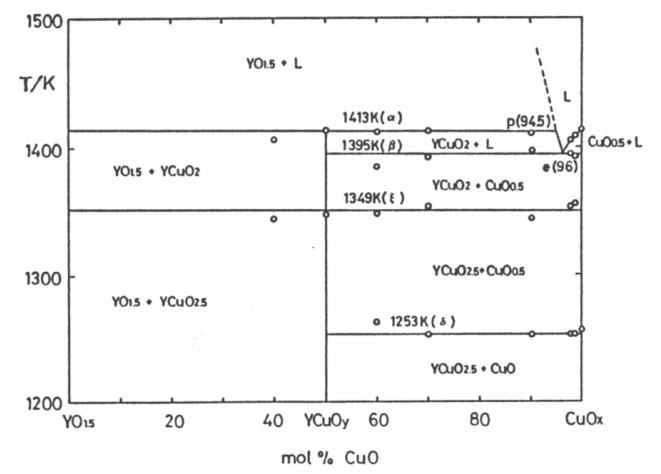

Fig. 9. Quasi-binary isobaric section of $YO_{1.5}$-CuO_x under 0.1 bar O_2 partial pressure.

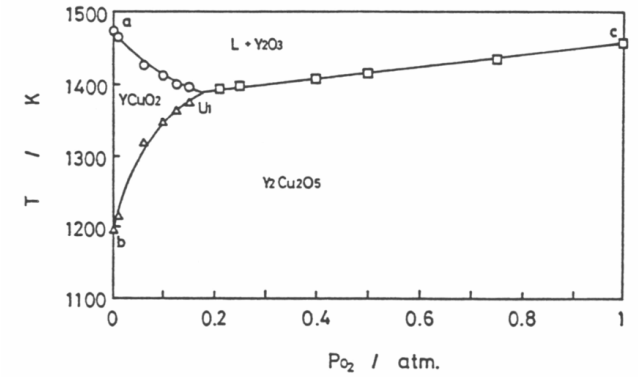

Fig. 12. Oxygen partial pressure dependence of the transition temperature and incongruent melting of the $Y_2Cu_2O_5$ and $YCuO_2$ compound.

Figure S7: Temperature-composition Cu-Y oxide phase diagram at 0.1 bar oxygen partial pressure (top), and temperature-oxygen pressure Cu-Y oxide phase diagram for Cu:Y (1:1) (bottom) (from Zhang *et al.*[39]).